International Journal of Advanced Research in Physical Science (IJARPS)
Volume 3, Issue 2, February 2016, PP 9-19
ISSN 2349-7874 (Print) & ISSN 2349-7882 (Online)
www.arcjournals.org

An Iterative Model of Performance of Micropixel Avalanche Photodiodes

A. Sadigov[a*], F. Ahmadov[a], S. Suleymanov[a], N.Heydarov[a], R.Valiyev[a], M.Nazarov[a], R. Akbarov[a], G. Ahmadov[b], Z. Sadygov[b], R. Madatov[c], R. Mechtiyeva[c], R. Mukhtarov[d], S. Khorev[e], F. Zerrouk[e]

[a] National Nuclear Research Center, Baku, Azerbaijan
[b]Joint Institute for Nuclear Research, Dubna, Moscow Region, Russia
[c] Institute Of Radiation Problems Of ANAS, Baku, Azerbaijan
[d]National Aviation Academy, Baku, Azerbaijan
[e]Zecotek Photonics, Inc.,Richmond, Bc, Canada
saazik@yandex.ru

Abstract: *An iterative model of the avalanche process in a micro-pixel avalanche photo-diode initiated by a single photo-electron is presented. The model describes development of the avalanche process in time, taking into account change of electric field within the depleted region caused by internal discharge and external recharge currents. Conclusions obtained as a result of modelling are compared with experimental data. Simulations show that typical durations of the front and rear edges of the discharge current have the same magnitude of less than 50 ps. The front of the external recharge current has the same duration; however duration of the rear edge depends on value of the quenching micro-resistor. It was found that effective capacitance of the pixel calculated as the slope of linear dependence of the pulse charge on bias voltage exceeds its real capacitance by a factor of two, while the total pixel voltage drop equals twice the value of bias over-voltage.*

Keywords: *Micropixel avalanche photodiode, MAPD, Silicon photomultiplier, SiPM, Micropixel photon counter, MPPC, Geiger-mode avalanche photodiodes, G-APD, Avalanche photodiode, APD.*

1. INTRODUCTION

Silicon micropixel avalanche photodiodes (MAPD) also known as Geiger-mode avalanche photodiodes (G-APD), micropixel photon counters (MPPC), and silicon photomultipliers (SiPM) are widely used as photo-detectors both in scientific and industrial applications [1]–[4]. Their general design proposed in [6] includes a matrix of small *p-n* junctions (pixels) with typical size of 10 to 100 µm created on the surface of a silicon substrate. These pixels are separated from each other by a certain space in order to eliminate charge coupling between them and each is connected to a common metal conduct through its individual microresistor with resistance of 10^5 to 10^6 Ω. The pixel area and the value of its microresistor are chosen so that the probability of spontaneous (dark) generation of charges in its active area is sufficiently small ($\ll 1$) over the time of electric relaxation of the pixel capacitance. This allows such pixel of the device to operate in overvoltage conditions, *i.e.* at reverse bias exceeding the breakdown voltage of the photodiode.

A great number of experimental and theoretical works (*e.g.* [7]–[16]) studied avalanche photodiode behaviour in overvoltage conditions. Authors of these papers explored mechanisms of formation of micro-plasma current pulses characterised with a typical flat top amplitude and random duration. The most comprehensive explanation of the physical origin of micro-plasma pulses was given by R. H. Haitz in [8].

The model described in [8] includes voltage source U_{br} (breakdown voltage of the photodiode), resistance R_{s} (resistance of the space charge region of the photodiode), and bi-stable switch S connected in series. Internal photodiode capacity C_{p} is connected in parallel to these components. In order to observe micro-plasma pulses, another voltage source with value of $U_{\mathrm{d}} > U_{\mathrm{br}}$ was connected to this circuit through a ballast resistor $R_{\mathrm{p}} \leq R_{\mathrm{s}}$. In this case, current pulses with a flat top and random duration emerge in the external circuit of the photodiode. The external charge current value J within

the flat top of these pulses is given by expression $J = (U_d - U_{br})/(R_p + R_s)$, while the potential difference U_p between the photodiode terminals is equal to $U_p = (U_d - J \times R_p) \geq U_{br}$. This means that a self-sustained avalanche process takes place inside the modelled photodiode with equal currents discharging (I) and charging (J). This mode of operation happens at relatively large values of current J (within the range of 50–100 μA depending on the device design) provided by voltage source U_d and ballast resistor R_p. In his follow-up article [9], R. H. Haitz further demonstrated experimentally that at sufficiently large values of ballast resistance R_p, it is possible to observe short photo signals of relatively constant amplitude and duration, but without any flat top. This mode of operation is usually referred to as Geiger mode. Of course, this mode of the device is not a self-sustained avalanche process, and therefore this process cannot be described with micro-plasma model. However, the author did not propose a corresponding model describing this mode of photodiode operation.

Single element avalanche photodiodes operating in Geiger mode, also known as single photon avalanche photodiodes (SPAD), as well as SiPM type devices have been thoroughly studied in [11]–[16] for photon counting applications. The authors of these publications introduced several new models (equivalent electrical circuits) of SPAD counters based on the original micro-plasma model proposed by R. H. Haitz. However, as it was mentioned above, Haitz's model cannot describe the Geiger-mode photodiodes because large values of resistance R_p ($R_p \gg R_s$) do not allow the device to reach the conditions of micro-plasma breakdown. Therefore, to provide a valid description of the avalanche parameters at Geiger-mode conditions, a new model of avalanche process needs to take into account development of the avalanche process occurring within the depleted region of the device at small recharge current values.

The present work proposes a new model of operation of devices such as SPAD and MAPD and compares the generated theoretical parameters with experimental data.

2. Model of Avalanche Process in Micro pixel Avalanche Photodiode

It is know that each pixel of the MAPD acting as an independent photodiode is connected to a common bias via its individual microresistor. Because of this, it is sufficient to consider operation of a single pixel for modelling to describe all device parameters. To simplify the following discussion, we will assume that the MAPD pixel has a p^+-i-n^+ structure with its individual quenching microresistor R_p (Figure1). Reverse bias voltage U_d applied to the pixel creates in the i-layer of thickness W a uniform electric field $E = E_d = U_d/W$ strong enough to start the avalanche process.

A single photo electron created within the i-layer near the pixel's anode (p^+-layer) creates electron-hole pairs on its way through entire thickness (W) of the i-layer. Due to the exponential character of avalanche process, the majority of these electron-hole pairs are created near the cathode (n^+-layer, Figure1a). The same behaviour is followed in avalanche processes initiated by a single hole. In this latter case, the majority of electron-hole pairs are created near the pixel anode (p^+-layer). This circumstance leads us to make a model assumption that the impact ionisation process takes place only in thin layers (thickness $d \ll W$) near the cathode and anode of the pixel. Gain factor for a single electron and a single hole was calculated as $M_e = \exp(\alpha W)$ and $M_h = \exp(\beta W)$ respectively. Here α and β are ionisation coefficients for electrons and holes. The following expressions were used to take into account dependence of α and β on electric field E [20]:

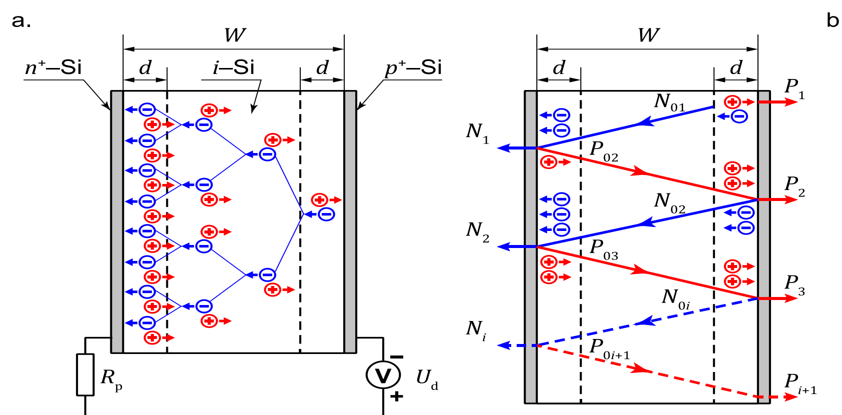

Figure1. *Schematic views of real avalanche process (a) model of operation (b) of a single MAPD pixel*

$$\alpha(E) = 3.8 \times 10^6 \times \exp\left(-\frac{1.75\times10^6}{E}\right), \quad \beta(E) = 2.25 \times 10^7 \times \exp\left(-\frac{3.26\times10^6}{E}\right), \tag{1}$$

where electric field E is in [V/cm] and α and β are in [1/cm].

Successive stages of the modelled avalanche process are shown schematically in Figure1*b*. One photo-electron is created near the anode ($N_{01} = 1$) at time $t = 0$. The electron passes through the i-layer and creates electron-hole pairs near the cathode. The time this process takes is $\tau = (W/v)$, where v is drift velocity which is equal to the thermal velocity of charge carriers in the i-layer. Here, we have taken into consideration the fact that high electric fields effectively lead to saturation of drift velocities of both electrons and holes when they reach their maximal value, in silicon equal to $v{\sim}10^7$ cm/s at room temperature. The number of electrons N_1 collected at the cathode, number of holes P_{02} moving toward the anode, and electric field E_1 during this step can be expressed as

$$N_1 = \exp(\alpha_1 W), P_{02} = [\exp(\alpha_1 W) - 1], \; E_1 = (U_1/W). \tag{2}$$

where $\alpha_1 = \alpha(E = E_1)$ and $U_1 = U_\mathrm{d}$.

The holes move towards the anode and create near it new electron-hole pairs after another period of time τ. All these holes are collected at the anode and a new number of electrons N_{02} start the second stage of the avalanche:

$$N_{02} = [\exp(\alpha_1 W) - 1] \times [\exp(\beta_1 W) - 1] \tag{3}$$

where $\beta_1 = \beta(E = E_1)$. And so, new electrons appear near the anode after every time period 2τ, starting a new stage of the avalanche.

There are two processes that affect electric field within the i-layer of the pixel. The first one is pixel discharge due to separation of electrons and holes and the second one is recharge of the pixel from an external power supply through the resistor R_p. Because of these processes, the second stage of the avalanche takes place at a different electric field strength $E = E_2 = U_2/W$ and different values of the ionisation coefficients $\alpha_2 = \alpha(E = E_2)$ and $\beta_2 = \beta(E = E_2)$. The new value of electric field is

$$E_2 = \frac{U_2}{W} = \frac{1}{W} \times \left[U_1 - \frac{qN_1 - \frac{U_\mathrm{d} - U_1}{R_\mathrm{p}} \times 2\tau}{C_\mathrm{p}}\right] \tag{4}$$

where q is the electron charge and C_p is the pixel capacitance. The value of the voltage drop due to the first stage of the avalanche is qN_1/C_p and the value of the voltage increase due to recharge from the external power supply with voltage U_d is $(U_\mathrm{d} - U_1)2\tau/R_\mathrm{p}C_\mathrm{p}$.

As a result, the number of electrons collected at the cathode after the second stage of avalanche process is

$$N_2 = N_{02} \times \exp(\alpha_2 W) = [\exp(\alpha_1 W) - 1] \times [\exp(\beta_1 W) - 1] \times \exp(\alpha_2 W) \tag{5}$$

Hence, the number of electrons collected at the cathode after the ith stage is

$$N_i = \{\textstyle\prod_{j=2}^{i} [\exp(\alpha_{j-1} W) - 1] \times [\exp(\beta_{j-1} W) - 1]\} \times \exp(\alpha_j W), \; i \geq 2 \tag{6}$$

and the electric field at the same time is

$$E_i = \left(\frac{U_i}{W}\right) = \frac{1}{W} \times \left[U_{i-1} - \frac{qN_{i-1} - \frac{U_\mathrm{d} - U_{i-1}}{R_\mathrm{p}} \times 2\tau}{C_\mathrm{p}}\right]. \tag{7}$$

Gain (M) of the MAPD pixel for a single initial photo electron can be calculated as

$$M = N_1 + \textstyle\sum_{i=2}^{\infty} N_i. \tag{8}$$

Expressions (2) and (6) allow one to investigate dependence of the internal discharge current due to the avalanche process $I_i(t_i) = qN_{i-1}/2\tau$ and the external recharge current $J_i(t_i) = (U_\mathrm{d} - U_{i-1})/R_\mathrm{p}$ at time $t_i = (i-1) \times 2\tau$. The time dependence of other parameters can be studied as well.

As it will be shown below, the proposed model can describe not only characteristics of MAPDs in Geiger mode (operating above the breakdown voltage) but also those of regular avalanche photodiodes operating below the breakdown voltage.

3. Calculation and Comparison with Experimental Data

One of the main MAPD parameters is its breakdown voltage U_{br}. It is defined as the minimum value of voltage applied between the cathode and anode of the pixel ($R_{\mathrm{p}} = 0$) at which the avalanche process initiated by a single electron has infinite number of cycles. The latter condition is met when at least one electron is created at the beginning of each avalanche cycle, or

$$N_{0i} = N_{i-1}[\exp(\alpha_{i-1}W) - 1] \times [\exp(\beta_i W) - 1] = 1. \qquad (9)$$

Numerical solution of equation (9) using $W = 1$ µm, $v = 10^7$ cm/s, $C_{\mathrm{p}} = 20$ fF, $R_{\mathrm{p}} = 220$ kΩ and and $\tau = (W/v) = 10$ ps gives $U_{\mathrm{br}} = 33.55$ V.

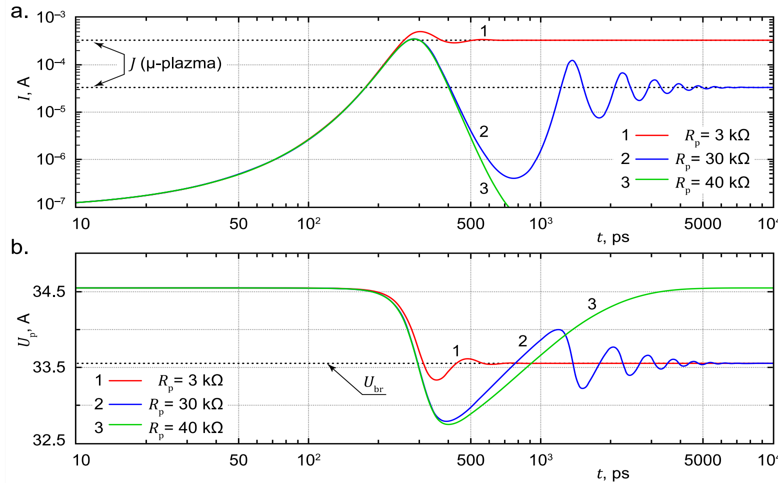

Figure2. *Temporal trace of the internal discharge current I (a) and the pixel voltage U_p (b) at values of the ballast resistor $R_p = 3$ kΩ (1), $R_p = 30$ kΩ (2), and $R_p = 40$ kΩ (3) and $C_p = const = 20$ fF*

Modelling results demonstrate that the mode of operation of an MAPD pixel depends both on the external voltage U_{d} and on the pixel capacitance C_{p}. At certain fixed values of the internal pixel capacitance C_{p} and overvoltage ΔU_{p}, there is a corresponding (low) value of resistance R_{p}, at which the triggered avalanche process becomes self-sustained, relatively quickly developing into a stationary current $I = J$, not unlike the already mentioned well-known microplasma breakdown in *p-n* transitions (see Figure2*a*, curve 1). At relatively large values of resistance R_{p}, a decaying transient oscillation of the current is observed (Figure2*a,* curve 2), also leading to the micro-plasma breakdown process, in which the conditions $U_{\mathrm{p}} = U_{\mathrm{br}}$ and $I = J$ hold true. In both these cases, the voltage on the pixel drops down to the breakdown value. This behaviour results from a high recharge current that does not let the pixel discharge below the breakdown voltage and quench the avalanche process. Even higher values of R_{p} lead to termination of the avalanche process and establish Geiger mode of operation (Figure2*a* and 2b, curve 3). This indicates existence of a certain threshold value R_{th} of the ballast resistor R_{p}, below which Geiger mode cannot be reached.

Physically, for the avalanche process to be quenched after the ith cycle (or at the moment $t_i = t_{\mathrm{q}}$), it is necessary that the average number of electrons N_{0i}, which initiate the following avalanche cycle, be inferior to one, that is:

$$N_{0i} = N_{i-1}[\exp(\alpha_{i-1}W) - 1] \times [\exp(\beta_i W) - 1] < 1. \qquad (10)$$

It was discovered that at a fixed breakdown voltage U_{br}, the introduced above threshold value R_{th} depends on the bias voltage U_{d} (or overvoltage) and the pixel capacitance C_{p}. As it can be seen from Figure3, the value of R_{th} reaches its maximum at bias voltage U_{d} close to the breakdown voltage U_{br} and then monotonically drops off at higher values of U_{d}. Physically, this non-trivial behaviour is caused by simultaneous discharging and charging processes, which depend differently on the overvoltage value. Of practical interest is the maximal value of R_{th}, which would guarantee that a pixel with capacitance of C_{p} and breakdown voltage of U_{br} may operate in Geiger mode at any bias voltage $U_{\mathrm{d}} > U_{\mathrm{br}}$. We will call this the critical value R_{cr} of the ballast resistor. Figure3 presents three different values of the critical resistance R_{cr} calculated for three values of the pixel capacitance $C_{\mathrm{p}} = 20, 40, 80$ fF and equal to 220, 155, and 110 kΩ correspondingly.

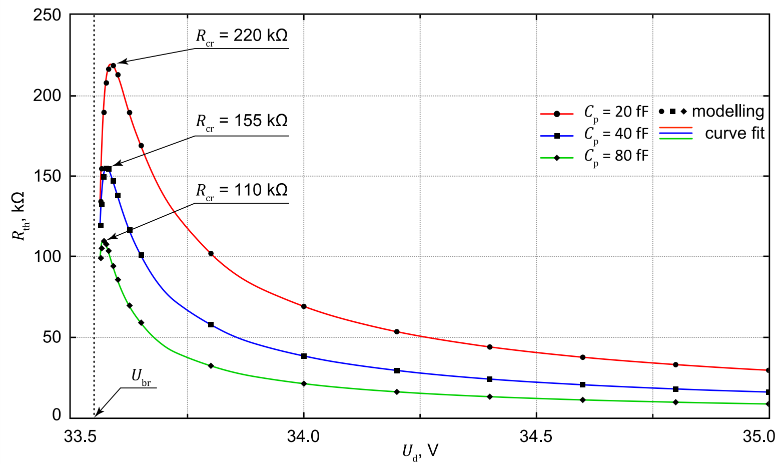

Figure3. *Dependence of the threshold resistance* R_{th} *upon voltage* U_d *applied to the pixel. Curves 1–3 correspond to capacitance* C_p *values of 20, 40, and 80 fF respectively*

Figure4 shows time dependence of the internal discharge current I (curve 1) and current in the external circuit J (curve 2). Internal discharge current profile I has the same values of both rise and fall times (about 44 ps at overvoltage $\Delta U_{\mathrm{p}} = 2$ V). The same value of the rise time is shared by the external current J. However, the fall time of the external current pulse J is three orders of magnitude longer. It is defined by the value of $C_{\mathrm{p}} \times R_{\mathrm{p}} \sim 4.4$ ns.

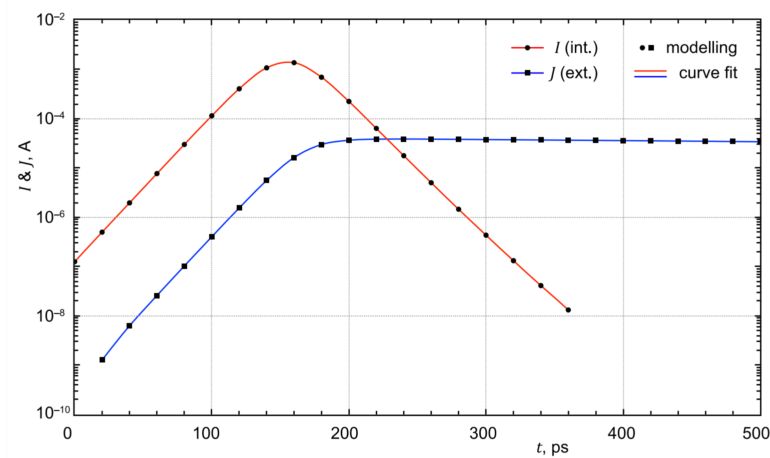

Figure4. *Shape of the MAPD pixel current pulse: internal avalanche current I (red curve) and external current J in the pixel circuit (blue curve)*

In order to understand the internal process of avalanche development, it is important to know number of electrons N_i created during each cycle of the avalanche process. Calculations show that the value of N_i rises sharply within a few cycles and reaches its maximum value $N_{max.} \approx 1.7 \times 10^5$ electrons. Thereafter, it falls at the same rate (Figure5a). During the same period, electric potential of the pixel U_{p} decreases, reaching level of U_{br} at the moment when the number of charge carriers N_i reaches its maximum $N_{max.}$. These charge carriers leads to further drop of pixel potential well below the breakdown voltage. As a result, the avalanche process is rapidly quenched. Figure5b shows that the total potential drop reaches $4\,\mathrm{V} = 2 \times \Delta U_{\mathrm{p}}$, where $\Delta U_{\mathrm{p}} = (U_{\mathrm{d}} - U_{\mathrm{br}})$ is overvoltage. The apparent ~10 ps shift of the moment $U_{\mathrm{p}} = U_{\mathrm{br}}$ in Figure5b illustrates limited precision of the proposed model coming from the fact that the current value at stage i is calculated from the parameters of the previous stage $(i - 1)$ of the avalanche process. Physically, the maximum number of charge carriers in the avalanche cycle must be reached at $U_{\mathrm{p}} = U_{\mathrm{br}}$.

The total charge of a single-electron pulse ($Q_{\mathrm{e}} = q \times M$) generated in an MAPD pixel is shown in Figure6 as a function of applied voltage U_{d}. Many people using the MAPD (or MPPC) devices believe that this linear dependence can be used to determine the pixel capacitance C_{p} taken to be equal to $C_{\mathrm{eff}} = \partial Q_{\mathrm{e}}/\partial U_{\mathrm{d}}$. However, our model demonstrates that this is not the case and $C_{\mathrm{eff}} = 2C_{\mathrm{p}}$. As a result, $Q_{\mathrm{e}} = C_{\mathrm{eff}} \times \Delta U_{\mathrm{p}} = C_{\mathrm{p}} \times 2\Delta U_{\mathrm{p}}$.

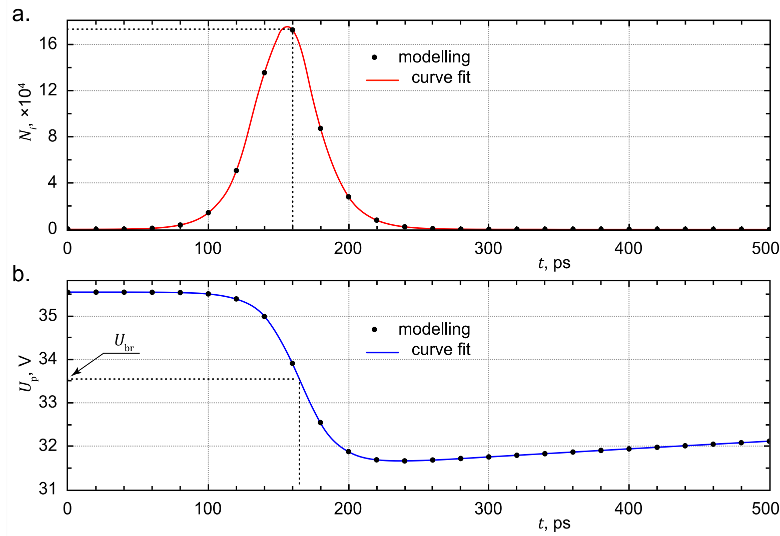

Figure5. *Time dependence of quantity of electrons N_i generated during avalanche cycles (a) and voltage drop U_p in the pixel (b)*

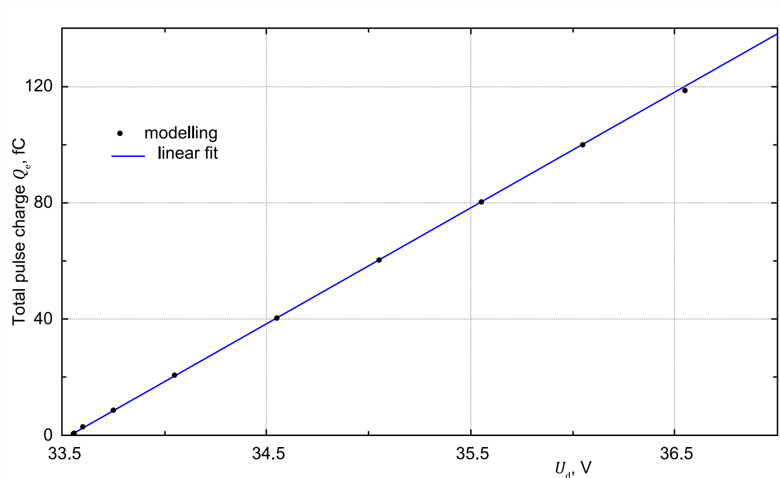

Figure6. *Dependence of total charge of a single-electron pulse on applied voltage ($C_p = 20\,fF$, $R_p = 220\,k\Omega$)*

Taking into account the preceding discussion of our results, it is possible to propose two new equivalent circuits of an avalanche photo-diode (pixel) operating in Geiger mode. The first equivalent circuit is an analogue of the original Haitz's model which comprises serially connected fictitious voltage source $U_0 = U_{\rm br} - \Delta U_{\rm p}$ (the minimal pixel voltage after quenching of avalanche process), resistance $R_{\rm s}$ (resistance of space charge region of the photodiode), and bi-stable switch S. The internal pixel capacitance $C_{\rm p}$ is connected in parallel to these components and the device is reverse-biased through ballast resistor $R_{\rm p}$ by voltage source $U_{\rm d} > U_{\rm br}$ (Figure7*a*). This model is distinguished from the original one proposed in [8] by a different value of the internal voltage source (the original model has $U_0 = U_{\rm br}$).

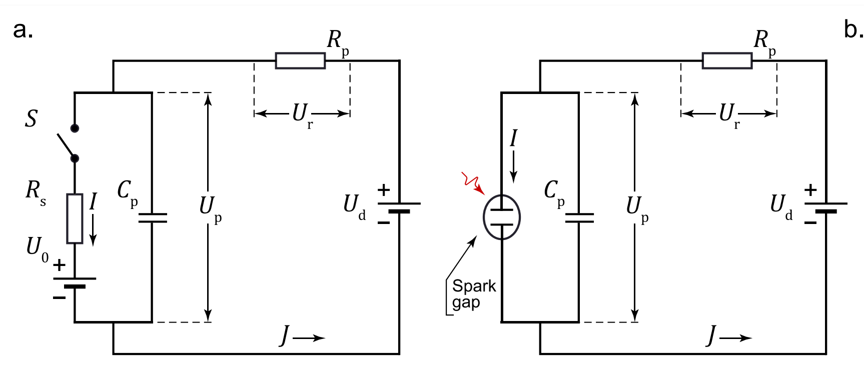

Figure7. *Equivalent circuits of a single MAPD pixel operating in Geiger mode*

The second equivalent circuit is based on our model discussed in the foregoing sections of this article. It is different from the previous one in that the avalanche photodiode (pixel) is now represented by the internal device capacitance C_p and a spark gap with external quenching resistor R_p (Figure7*b*). The operation of this spark gap is governed by Equations (6)–(8).

In order to model various types of micropixel avalanche photodiodes, the proposed circuits may be complemented with additional necessary elements (serial resistors, shunting capacitances, &c). However, within the scope of the present work, we limit our comparative analysis to the above-discussed circuits.

We consider that the bi-stable element S is switched on at moment $t=t_0$. Applying the Kirchhoff's rules to the equivalent circuit of Figure7*a*, we arrive at the equations for the dependence of the pixel voltage U_p and the external current J upon time:

$$U_d = U_p + U_r;\ J = \frac{U_r}{R_p};\ I = \frac{U_p - U_0}{R_s}. \tag{11}$$

In the preceding Equation (11), U_r is the voltage drop over resistor R_p, $U_0 = U_d - \Delta U_p$, and ΔU_p is the overvoltage value. Additionally, voltage U_p may be expressed in terms of charge Q_p accumulated in capacitor C_p:

$$U_p = \frac{Q_p}{C_p} = \frac{1}{C_p} \times \left(C_p \times U_d - \int_0^t I \times dt' + \int_0^t J \times dt'\right). \tag{12}$$

Differentiating Equation (12) and replacing I and J with their expressions from Equation (11), we will obtain:

$$\frac{dU_p}{dt} = -\frac{U_p}{\tau_r} + \frac{U_{st}}{\tau_r};\ U_p(t=0) = U_d, \tag{13}$$

where $U_{st} = \frac{U_0 \times R_p + U_d \times R_s}{R_p + R_s}$ is the stationary value of U_p after switch S makes the circuit (i.e. at $t \to \infty$), $\tau_r = R_o \times C_p$, and $R_o = \frac{R_p \times R_s}{R_p + R_s}$. By solving Equation (13), one can derive the following formulae for dependence of U_p and J upon time:

$$U_p(t) = U_{st} + (U_d - U_{st}) \cdot \exp\left(-\frac{t}{\tau_r}\right), \quad J(t) = \frac{U_d - U_{st}}{R_p} \times \left[1 - \exp\left(-\frac{t}{\tau_r}\right)\right]. \tag{14}$$

Figure8 demonstrates the results of calculations based on two equivalent circuits proposed in Figure7. The value of R_s was chosen so as to produce similar duration of the rise edges of photo current pulses generated in the proposed circuits (around 40 ps). Here, we analyse the case when the avalanche process is triggered in both circuits simultaneously at $t_0 = 20$ ps.

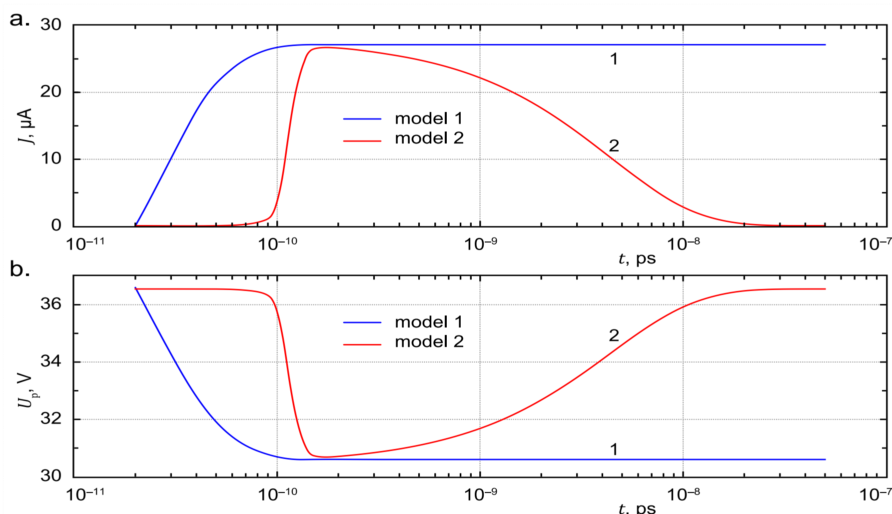

Figure8. *Temporal dependence of the external photo current and pixel voltage calculated on the basis of the first (curve 1) and second (curve 2) equivalent circuits at* $U_{br} = 33.55$ *V,* $\Delta U_p = 3$ *V,* $C_p = 20$ *fF,* $R_p = 220$ *kΩ, and* $R_s = 1$ *kΩ*

It can be seen that the first of the discussed equivalent circuits is only adequate for description of the front edge of the photo-response, following which the external current reaches a certain stationary value. The pixel voltage drops below the breakdown voltage by the overvoltage value and remains at this level. Furthermore, the first of the proposed circuits does not produce a certain delay in formation

of the photo current pulse. This indicates that no equivalent circuit of this type can adequately describe the process of formation of a single electron photo current pulse in MAPD. The second equivalent circuit (Figure7*b*) obviously does not suffer from these limitations. This latter circuit demonstrates the entire process of formation of a single electron avalanche photo current with subsequent quenching of the avalanche process and restoration of the initial pixel voltage (curve 2 in Figure8).

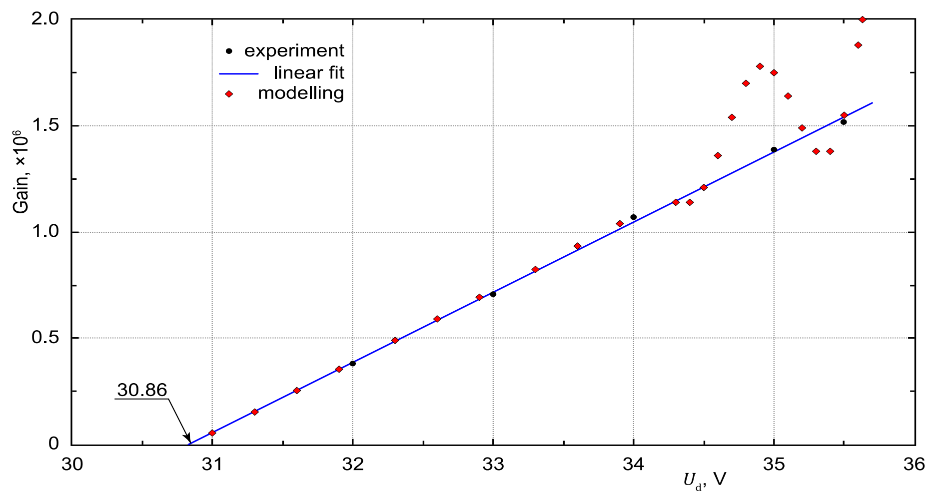

Figure9. *Gain of a single-pixel avalanche photo-diode as a function of the bias voltage*

In the following discussion, the results of our simulations are compared with some experimental data. It should be noted that our simple model does not take into account possible non-uniformity of electric field inside the experimental devices. However, various Geiger-mode devices demonstrate similar behaviour at the same overvoltage value ΔU_{p}. In our calculations, we selected model parameters so as to produce breakdown voltages close to those of the experimental devices. Figure9 shows an experimental gain-voltage dependence of a single pixel avalanche photodiode with an integrated individual microresistor (data taken from [21]). The value of the pixel's capacitance determined from the dependence slope is $C_{\mathrm{eff}} = 54$ fF. However, no experimentally measured data on pixel capacitance are given in [21]. In order to find the terminal capacitance of this device we used the effective pixel size (34×34 μm^2) and thickness of the depletion region (4 μm). Our calculation (in the approximation of a flat capacitor with no edge effects) based on these pixel dimensions taken from [21] gives a value of $C_{\mathrm{p}} = 30.4$ fF $\approx C_{\mathrm{eff}}/2$, which is predicted by the proposed model of avalanche process.

Results of modelling at $U_{\mathrm{br}} = 30.86$ V and $C_{\mathrm{p}} = 30.4$ fF are also presented in Figure9. One can see that the proposed model describes the experimental data reasonably well up to $U_{\mathrm{p}} = 34$ V (equivalent to overvoltage value of $\Delta U_{\mathrm{p}} = 34 - 30.86 \approx 3$V). Considerable discrepancy of modelling and the experimental data at $U_{\mathrm{p}} > 34$ V arises from rapid increase of both electron and hole ionisation coefficients within the avalanche region. The pixel is discharged considerably in very few multiplication cycles, stopping the avalanche process. Rapidity of quenching is driven by the number of charge carriers produced in the last avalanche cycle, in which $U_{\mathrm{p}} \geq U_{\mathrm{br}} = 30.86$ V. Since in order to calculate the number of carriers in each cycle of the avalanche process (N_i), the data from the preceding cycle (N_{i-1}) are used, limited number of cycles leads to substantial deviation from the experimental data, including apparent oscillations in the dependence of gain upon bias.

We also studied our SPAD-type device fabricated together with Zecotek Photonics, Inc. (www.zecotek.com), which consisted of two elements: a small-area photodiode and an external quenching resistor $R_{\mathrm{p}} = 200$ kΩ. Both of these elements were mounted on a PCB (printed circuit board) plate. The small area photodiode was fabricated on the basis of a 3 μm thick epitaxial silicon layer with n-type conductivity grown on surface of a silicon substrate having n-type conductivity. Specific resistance of the substrate and the epitaxial layer was 0.05 and 30 Ω·cm respectively. The active and contact areas of the photodiode were 100×100 and 160×160 μm correspondingly. The contact area was wire bonded to the quenching resistor R_{p}. Total terminal capacitance of this SPAD device was $C_{\mathrm{p}} = 1.3$ pF.

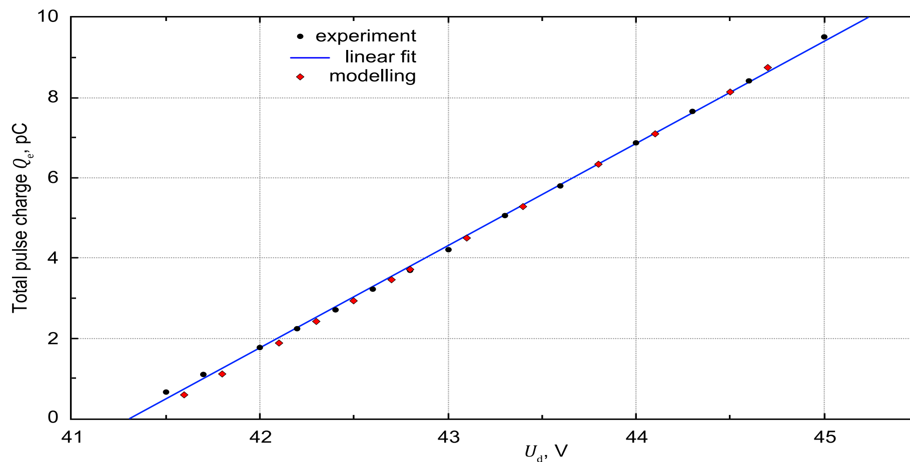

Figure10. *Charge of single photoelectron pulses as a function of the bias voltage measured in the Zecotek device*

Figure10 shows dependence of the single photoelectron charge upon the applied voltage. One can see that results of our modelling demonstrate good agreement with the experimental data. Calculated from the line slope, effective pixel's capacitance is $C_{\text{eff}} = 2.7$ pF, which is approximately twice the value of the measured pixel capacitance $C_{\text{p}} = 1.3$ pF.

4. Conclusion

The developed iterative model allows one to simulate operation of avalanche photodiodes in Geiger mode. It gives correct qualitative behaviour of MAPD parameters as a function of applied voltage.

Simulations show that typical duration of the front and rear edges of the discharge current are of the same magnitude, which is shorter than 50 ps at overvoltage value $\Delta U_{\text{p}} = 2$ V. The leading front of the external recharge current is also of the same magnitude.

One of the important results obtained from this model is a description of the avalanche process behaviour when the pixel potential reaches the value of the breakdown voltage. The pixel potential then continues dropping and new electron-hole pairs are being produced at a decreasing rate. The number of charge carriers produced after the voltage drops below the breakdown voltage is approximately the same as the number of those produced above the breakdown voltage. As a result, the potential on the pixel drops below the breakdown voltage by the overvoltage value ΔU_{p}, and effective pixel capacitance calculated as the slope of linear dependence of the pulse charge on bias voltage is about two times greater than its terminal capacitance.

Acknowledgements

This work is supported by Science Development Foundation under the President of the Republic of Azerbaijan (Grant № EIF-2014-9 (24) -KETPL-14/03/1).

References

[1] Z. Sadygov, A. Olshevski, I. Chirikov, I. Zheleznykh, and A. Novikov; *Nucl. Instrum. Meth. A* 567 70 (2006).

[2] Y. Musienko, S. Reucroft, and J. Swain; International workshop on new photon-detectors PD07 (2007).

[3] D. Renker and E. Lorenz; JINST 4 P04004 (2009).

[4] Z. Sadygov, A. Ol'shevskii, N. Anfimov, T. Bokova, A. Dovlatov, V. Zhezher, Z. Krumshtein, R. Mekhtieva, R. Mukhtarov, M. Troitskaya, V. Chalyshev, I. Chirikov-Zorin, V. Shukurova; Technical Physics Letters 36 528 (2010).

[5] N. Anfimov, I. Chirikov-Zorin, A. Dovlatov, O. Gavrishchuk, A. Guskov, N. Khovanskiy, Z. Krumshtein, R. Leitner, G. Meshcheryakov, A. Nagaytsev, A. Olchevski, T. Rezinko, A. Sadovskiy, Z. Sadygov, I. Savin, V. Tchalyshev, I. Tyapkin, G. Yarygin, F. Zerrouk; Nucl. Instrum. Meth. A 617 78 (2010).

[6] Z. Sadygov, *Russian Patent #2102820*, priority of 10.10.1996.

[7] R. J. McIntyre; J. Appl. Phys. 32, pp. 983–995, (1961).

[8] R. H. Haitz; J. Appl. Phys. 35, pp. 1370–1376, (1964).

[9] R. H. Haitz; J. Appl. Phys. 36, pp. 3123–3131, (1965).

[10] W. G. Oldman, R. R. Samuelson, P. Antognetti; IEEE Trans. Electron Dev. 19, pp. 1056–1060, (1972).

[11] S. Cova, A. Longoni, and A. Andreoni; Rev. Sci. Instrum., 52, pp. 408–412, (1981).

[12] S. Cova, A. Longoni, A. Adreoni, and R. Cubeddu; IEEE J. Quantum Electron., 19, pp. 630–634, (1983).

[13] S. Cova, A. Lacaita, M. Ghioni, G. Ripamonti, and T. A. Louis; Rev. Sci. Instrum., 60, pp. 1104–1110, (1989).

[14] H. Dautet, P. Deschamps, B. Dion, A. D. MacGregor, D. MacSween, R. J. McIntyre, C. Trottier, and P. P. Webb; Appl. Opt. 32, pp. 3894–3900, (1993).

[15] A. Lacaita, M. Ghioni, F. Zappa, G. Ripamonti, and S. Cova; Nucl. Instrum. Methods, A 326, pp. 290–294, (1993).

[16] S. Cova, M. Ghioni, A. Lacaita, C. Samori, F. Zappa; Appl. Optics 35, pp. 1956-1976, (1996).

[17] F. Corsi, A. Dragone, Marzocca, A. Del Guerra, P. Delizia, N. Dinu, C. Piemonte, M. Boscardin, G.F. Dalla Betta Nucl. Instrum. Meth. A 572, pp. 416-418, (2007).

[18] H. Otono, H. Oide, S. Yamashita, and T. Yoshioka; Nucl. Instrum. Meth. A 610, pp. 397-399, (2009).

[19] S. Seifert, H.T. van Dam, J. Huizenga, R. Vinke, P. Dendooven, H. Lohner, D.R. Schaart; IEEE Trans. on Nucl. Science 56, 3726, (2009).

[20] C. A. Lee, R. A. Logan, R. L. Batdorf, J. J. Kleimack, and W. Wiegmann; Phys. Rev. 134 (1964) A761.

[21] C. Piemonte, R. Battiston, M. Boscardin, G.-F. Dalla Betta, A. Del Guerra, N. Dinu, A. Pozza, N. Zorzi; *IEEE Trans. on Nucl. Science* 54, 236, (2007).

AUTHORS' BIOGRAPHY

Sadygov Azar, is a PhD student (Physics) working as an engineer in the Department of Instrumental Engineering and Innovation is affiliated with Ministry of Communication and High Technologies-National Nuclear Research Centre.

Ahmadov Farid Ph.D, is the Head of Department of Instrumental Engineering and Innovation is affiliated with Ministry of Communication and High Technologies-National Nuclear Research Centre.

Suleymanov Samir, is a PhD student (Physics) and he is currently working as an engineer in the Department of Instrumental Engineering and Innovation is affiliated with the Ministry of Communication and High Technologies-National Nuclear Research Centre

Heydarov Namiq, is a PhD student (Physics) and he is currently working as an Engineer in the Department of Instrumental Engineering and Innovation is affiliated with the Ministry of Communication and High Technologies-National Nuclear Research Centre

Valiyev Rusif, is a PhD student (Physics) and he is currently working as an Engineer in the Department of Instrumental Engineering and Innovation is affiliated with the Ministry of Communication and High Technologies-National Nuclear Research Centre.

Nazarov Magsud, is a PhD student (Physics) and he is currently working as an Engineer in the Department of Instrumental Engineering and Innovation is affiliated with the Ministry of Communication and High Technologies-National Nuclear Research Centre.

Akberov Ramil, is a PhD student (Physics) and he is currently working as an Engineer (Department of Instrumental Engineering and Innovation is affiliated with the Ministry of Communication and High Technologies-National Nuclear Research Centre.

Ahmadov Gadir PhD, is currently working as a Junior scientific researcher in the Frank Laboratory of Neutron Physics is affiliated with the Joint Institute for Nuclear Research

Sadygov Ziraddin, is a Doctor of Phys.-Math. Sciences and he is currently working as a Senior scientific researcher in Veksler and Baldin Laboratory of High Energies and is affiliated with the Joint Institute for Nuclear Research

Madatov Rahim, is a Doctor of Phys.-Math. Sciences and he is currently working as a Head of laboratory of Radiation Physics of Semiconductors is affiliated with the Institute of Radiation Problems of ANAS.

Mechtiyeva Ravan, Ph.D. in Physics and Mathematics is currently working as a Deputy Director on Scientific Works Institute of Radiation Problems of ANAS

Mukhtarov Ramil, PhD in Technical Sciences is currently working as a junior scientific researcher in the Department of Aviation Security is affiliated with the National Aviation Academy